SPE 166447

Modeling Low Salinity Waterflooding: Ion Exchange, Geochemistry and Wettability Alteration

Cuong .T.Q. Dang, University of Calgary, Long .X. Nghiem, Computer Modeling Group Ltd., Zhangxin Chen, University of Calgary, Quoc .P. Nguyen, The University of Texas at Austin

This paper was prepared for presentation at the SPE Annual Technical Conference and Exhibition held in New Orleans, Louisiana, USA, 30 September–2 October 2013.

Abstract

Low salinity waterflood (LSW) has become an attractive enhanced oil recovery (EOR) method as it shows more advantages than conventional chemical EOR methods in terms of chemical costs, environmental impact, and field process implementation. Extensive laboratory studies in the past two decades have proposed several pore-scale mechanisms of oil displacement during LSW flooding, which are still open for discussion. However, the capability of reservoir simulators to model accurately this process is very limited. This paper provides a critical review of the state of the art in research and field applications of LSW. The focus is on a widely agreed mechanism that is the wettability alteration from preferential oil wetness to water wetness of formation rock surfaces. Ion exchange and geochemical reactions have been experimentally found to be important in oil mobilization due to enhanced water spreading at low salinity. To evaluate the significance of this surface wetting mechanism, a comprehensive ion exchange model with geochemical processes has been developed and coupled to the multi-phase multi-component flow equations in an equation-of-state compositional simulator. This new model captures most of the important physical and chemical phenomena that occur in LSW, including intra-aqueous reactions, mineral dissolution/precipitation, ion exchange and wettability alteration.

The proposed LSW model is tested using the low-salinity core-flood experiments reported by Fjelde et al. (2012) for a North Sea reservoir and the low-salinity and high-salinity heterogeneous core-flood experiments by Rivet (2009) for a Texas reservoir. Excellent agreements between the model and the experiments in terms of effluent ion concentrations, effluent pH, and oil recovery were achieved. In addition, the model was also proved to be highly comparable with the ion-exchange model of the geochemistry software PHREEQC for both low salinity and high salinity (Appelo, 1994). Important observations in laboratory and field tests such as local pH increase, decrease in divalent effluent concentration, mineralogy contributions, and the influence of connate water and injected brine compositions can be reproduced with the proposed LSW model. Built in a robust reservoir simulator, it serves as a powerful tool for LSW design and the interpretation of process performance in field tests.

Introduction

Low salinity waterflooding (LSW) is an emerging EOR technique in which the salinity of the injected water is controlled to improve oil displacement efficiency without a significant loss of infectivity due to clay swelling. In particular, the presence of clay minerals is a favorable condition for the high efficiency of this process. This recovery concept is quite attractive as 50% of the world's conventional petroleum reservoirs are found in sandstones that commonly contain clay minerals.

It has been experimentally found that changes in the injected brine composition can improve waterflood performance by up to 38% (Larger et al. 2004, Web et al. 2004), leading to a new concept of optimal injection brine composition for water flood. In the 1990s, Jadhunandan and Morrow (1995) and Yildiz and Morrow (1996) reported the influence of brine composition on oil recovery, which identified a possibility to improve waterfloods with optimized injection brine formulation. Numerous laboratory experiments (Tang and Morrow, 1997; Morrow

et al., 1998; Tang and Morrow, 1999; Tang and Morrow, 1999b; Zhang and Morrow, 2006; Zhang et al., 2007; Buckley and Morrow, 2010; Kumar et al., 2010; Lohardjo et al, 2010; Morrow and Buckley, 2011) have later confirmed that EOR can be obtained in tertiary low salinity waterflood. The salinity in these tests was in the range of 1,000-2,000 ppm. Although the advantages of LSW have been realized, the mechanism of incremental oil recovery by LSW is still an open discussion. Several mechanisms have been proposed during last two decades including fines migration, wettability alteration, multi-component ionic exchange (MIE), saponification and pH modification, and electrical double layer effects. Dang et al. (2013) provided a critical review of these mechanisms.

Fines migration is one of the first explanations for the incremental oil recovery by LSW. Morrow and his research colleagues observed that fines (mainly kaolinite clay fragments) were released from the rock surface, resulting in an increase of spontaneous imbibition recovery with a decrease in salinity for different sandstones. The fines migration was believed to improve mobility control of the conventional high salinity waterflooding by plugging pore throat and reduction in the effective permeability to water in the water swept zone and divert flow into un-swept zones. However, numerous researchers from industry (Larger et al., 2007, 2008a, 2008b; Webb et al., 2004, 2005, 2008; McGuire et al., 2005; Jerauld et al., 2008) reported that LSW has higher recovery without any observations of fines migration during their experiments and pilot tests. Based on these observations, people questioned about the link between fines migration and the additional oil recovery and it is not the direct cause for the benefits of LSW.

In fact, a local increase of pH is usually observed during LSW (McGuire et al., 2005; Larger, 2006, Zhang and Morrow, 2006, and Austad et al., 2010), and it is suggested that the EOR mechanisms of LSW appear similar to the alkaline flooding by generation of in-situ surfactants and reduction in the interfacial tension. Note that the acid number of crude oil should be larger than 0.2 mg KOH/g in order to generate enough surfactant to induce wettability reversal and/or emulsion formation in alkaline flooding (Ehrlcih et al., 1974; Jensen and Radka, 1988), but most of crude oil samples have been used with acid number less than 0.05 mg KOH/g for LSW experiments. Therefore, it is difficult to conclude that additional oil recovery is mainly from in-situ surfactant generation.

Among the proposed hypotheses, wettability alteration towards increased water wetness during the course of LSW is the widely suggested case of increased oil recovery. The effects of low salinity brine on wettability modifications have been reported by many authors (Jadunandan and Morrow, 1995; Tang and Morrow, 1999; Drummond and Isralachvili, 2002 and 2004; Vledder et al., 2010; Zekri et al., 2011). It has been experimentally found that the low salinity brine has a significant effect on the shape and the end points of the relative permeability curves (Webb et al., 2004; Kulkarni and Rao, 2005; Rivet, 2009; Fjelde et al., 2012), resulting in a lower water relative permeability and higher oil relative permeability. This phenomenon could be physical explained by the ionic exchange between the injected brine and formation water, and mineral dissolution/precipitation in LSW. The ionic exchange during this process leads to the adsorption of divalent ions, promotes the mineral dissolution, and changes the ionic composition of formation water and the wettability condition. This is the most reliable suggestion for the underlying mechanisms of LSW and it is used to develop a mechanistic model of LSW in this paper.

LSW has been evaluated at the field scale based on promising results from laboratory experiments (McGuire et al. 2005; Larger et al., 2008; Skrettingland et al., 2010; Thyne and Gamage, 2011). A summary of LSW field implementations is shown in Table 1. McGuire et al. (2005) and Larger et al. (2008) reported for the LSW performance in Alaska's oil fields using water injection salinity between 1,500 to 3,000 ppm. Based on single well chemical tracer tests (SWCTT), the reported incremental LSW EOR in these oil fields ranged from 6 to 12% OOIP, resulting in an increase in waterflooding recovery by of 8 to 19%. Lager et al. (2006) indicated that fines migration or significant permeability reduction due to LSW was never observed. He also achieved a 40% increase in recovery using a North Sea crude oil with very low acid number (Acid Number < 0.05). Another result from the Log-Inject-Log test (Webb et al., 2004) showed 25-50% reduction in residual oil saturation by LSW. Another successful LSW by SWCTT test was described by Seccombe et al. (2010) in a mature offshore oil field located on the North Slope of Alaska. Additionally, historical field evidence in the Powder River basin of Wyoming reported by Robertson (2010) also showed that oil recovery tended to increase by about 12.4% as the salinity of injection brine decreases. Thyne and Gamage (2011) published a comprehensive evaluation of the effect of LSW for 26 field trials in Wyoming.

Table 1: Summary of LSW Implementation in the Field

Author	Reservoir	Injected Brine (ppm)	Formation Damage	Incremental Oil Recovery (%)
Webb (2004)	Sandstone	3,000/ 220,000	No	20% -50%
McGuire (2005)	Sandstone <Alaska North Slope>	150-1,500 /15,000	No	13%
Robertson (2007)	Sandstone <West Semlek Reservoir> <North Semlek Reservoir> <Moran Reservoir>	10,000/60,000 3,304/42,000 7,948/128,000	No	Recovery tends to decrease as the salinity ratio increases.
Lager (2008)	Sandstone <Alaskan Oil Field>	2,600/ 16,640	No	10%
Veledder (2010)	Sandstone <Omar Oil Field> <Isa Oil Field>	2,200/ 90,000	No	10% - 15%
Seccombe (2010)	Sandstone <Endicot Oil Field>	12,000/ --	No	13%
Skrettingland (2010)	Sandstone <Snorre Oil Field>	500/50,000	No	No significant change.

While extensive experimental studies of LSW have been reported, modeling work is rarely found in the literature. One of the earliest studies on modeling LSW was presented by Jerauld et al. (2008). They developed a new model for LSW with some modifications from the traditional waterflooding model. In their model, salt was modeled as an additional single-lumped component in the aqueous phase, and relative permeability and capillary pressure are made functions of salinity, including the influence of connate water, hysteresis in water relative permeability between imbibitions, and dispersion phenomena. Unfortunately, this model used a simple linear dependence of residual oil saturation on salinity.

Rueslatten et al. (2008) performed a LSW experiment on a North Slope core sample. Then a model using the geochemical code, PHREEQC, was created to simulate the LSW. This model gave only an approximation of the pH variation as the mechanism of LSW. Subsequently, Sorbie and Collins (2010) extended their work by introducing a semi-quantitative model that describes the multicomponent ion exchange process at the pore scale. This model attempts to show the consequences of the change in the electrical double layers and the adsorption of polar organic species. However, further experimental studies are required to confirm this mechanism.

Recently, Omekeh et al. (2012) presented a model of ion exchange and mineral solubility in LSW. They considered two-phase flow of oil and brine that contains Na^+, Mg^{++}, SO_4^{--}, and Cl^-. Cations are involved in a fast ion exchange process with the negative clay surface, X^-. In this model, the total release of divalent cations from the rock surface gives rise to change of the relative permeability such that more oil is mobilized and the desorption of divalent ions is the main mechanisms of LSW. However, divalent ions such as Ca^{++} and Mg^{++} are expected to be adsorbed on the clay mineral during the course of LSW (Appelo, 1994) and the wettability alteration happens with the adsorption of divalent ions only (Suijkerbuijk et al. 2012). And it would be more advantageous to model the process in a compositional simulator with full geochemical reactions instead of in a simplified two phases flow model.

Since the capability of reservoir simulators to model accurately this process is limited, a comprehensive ion exchange model with geochemical processes including intra-aqueous and mineral reactions has been developed

and coupled to the multi-phase multi-component flow equations in an equation-of-state compositional simulator, Computer Modeling Group's GEM™. This new model captures most of the important physical and chemical phenomena that occur in LSW, including intra-aqueous reactions, mineral dissolution/precipitation, ion exchange and wettability alteration. The focus of this model is on the widely agreed mechanism that is the wettability alteration from preferential oil wetness to water wetness of formation rock surfaces due to ion exchange and geochemical reactions. Simulation results of laboratory LSW in linear core was carried out and validated against experimental data and compared with the geochemistry software PHREEQC. Mechanistic simulations not only provide a comprehensive comparison with the laboratory observations, but also give insights into the propagation of aqueous ions in the core and aid in future experiment setup and field scale LSW designs. Using numerical models, the LSW can be designed and optimized to promote the wettability alteration towards more water wetness condition for additional oil recovery.

Modeling of Low Salinity Waterflooding

Governing Equations

The flow in porous media is governed by Darcy's law and the mechanical dispersion/diffusion of components. The conservation equations for the species in a compositional model are described as follows.

The conservation equations of the n_h components in the oil and gas phases that may be soluble in the aqueous phase are:

$$\psi_i \equiv \sum_{\alpha=o,g,w} \Delta T^u_\alpha y^u_{i\alpha}\left(\Delta p^{n+1} + \Delta P^u_{c\alpha} - \tilde{\rho}^u_\alpha g \Delta d\right) + \sum_{q=g,o,w} \Delta D^u_{iq} \Delta y^u_{iq} + V\sigma^{n+1}_{i,aq} + q^{n+1}_i - \frac{V}{\Delta t}\left(N^{n+1}_i - N^n_i\right) = 0, \quad i = 1,...,n_h; \tag{1}$$

The conservation equations for the n_a aqueous components (ions) are:

$$\psi_j \equiv \Delta T^u_w y^u_{jw}\left(\Delta p^{n+1} - \tilde{\rho}^u_w g \Delta d\right) + \Delta D^u_{iw} \Delta y^u_{iw} + V\sigma^{n+1}_{j,aq} + V\sigma^{n+1}_{j,mn} + q^{n+1}_j - \frac{V}{\Delta t}\left(N^{n+1}_{ja} - N^n_{ja}\right) = 0, \quad j = 1,...,n_a \tag{2}$$

The conservation equations for the n_m mineral components are:

$$\psi_k \equiv V\sigma^{n+1}_{k,mn} - \frac{V}{\Delta t}\left(N^{n+1}_k - N^n_k\right) = 0, \quad k = 1,...,n_m. \tag{3}$$

The superscripts n and n+1 denote the old and new time levels, respectively. These equations are discretized in an adaptive implicit manner. The superscript u = n is for explicit gridblocks and n+1 for implicit gridblocks. The terms ($V\sigma^{n+1}_{k,mn}$) and ($V\sigma^{n+1}_{i,aq}$) correspond, respectively, to the intra-aqueous reaction rates and mineral dissolution/precipitation rates and will be discussed in the next section of this chapter.

The equation for thermodynamic equilibrium is the equality of fugacities of the components between the oil, gas and aqueous phases, i.e.,

$$g_{i,1} \equiv f_{ig} - f_{io} = 0, \ i = 1,...,n_h, \tag{4}$$

$$g_{i,2} \equiv f_{ig} - f_{iw} = 0, \ i = 1,...,n_h, \tag{5}$$

The fugacity f_{ig} is calculated from the Peng-Robinson equation of sate. The fugacity f_{iw} of gaseous components soluble in the aqueous phase is calculated using Henry's law, i.e.,

$$f_{iw} = y_{iw} H_i \tag{6}$$

In compositional simulation, a volume constraint equation is normally also a part of the equation set:

$$\sum_q \left(\frac{N^{n+1}_q}{\rho^{n+1}_q}\right) - \phi^{n+1} = 0, \ q = g,w,o. \tag{7}$$

Intra-aqueous and Mineral Reactions

Nghiem et al. (2004) proposed a fully-coupled geochemical Equation-of-State model for the simulation of CO_2 storage in saline aquifer in a compositional simulator. It allows the modeling of intra-aqueous reactions in the aqueous phase and reactions between minerals and aqueous species. Although this model was initially designed for the simulation of CO_2 storage, it is also applicable to the modeling of geochemical reactions in the LSW process. Nghiem et al.'s model has been extended to model LSW, which includes multiple-ion exchange and wettability alteration in addition to intra-aqueous chemical reactions and mineral dissolution and precipitation.

A chemical reaction is in equilibrium if the forward reaction-rate and backward reaction rates are equal giving a net reaction-rate of zero. Reactions in equilibrium satisfy the following condition:

$$Q_\alpha - K_{eq,\alpha} = 0 \ , \alpha = 1,\ldots,R_{aq} \tag{8}$$

$$Q_\alpha = \prod_{k=1}^{n_{aq}} (a_k)^{\nu_{k\alpha}} \tag{9}$$

Q_α is the activity product of a reaction where n_{aq} is the number of species in an intra-aqueous equilibrium reaction, a_k is the activity of each species in the aqueous phase, K_{eq} is the equilibrium constant for the chemical reaction, R is the universal gas constant, T is the fluid temperature, and $\nu_{k\alpha}$ is the stoichiometric coefficient of a component in the chemical reaction. The chemical equilibrium constant (K_{eq}) values are provided as a function of temperature for many aqueous reactions by Bethke (1996) or Kharaka et al. (1989).

Activities for each species (α_k) are related to their concentration (m_k) in solution. The activities of water and the mineral species can be taken to be unity without introducing significant errors (Helgeson *et al.*, 1970).

$$\alpha_i = \gamma_i m_i \quad i = 1,\ldots, n_{aq} \tag{10}$$

where γ_i is the activity coefficient. The activity coefficient in ideal cases can be taken to be approximately equal to the concentration of the species (in molality).

Intra-aqueous reactions are modeled as instantaneous reactions. This increases the computational efficiency by permitting the use of an Equilibrium-Rate-Annihilation (ERA) matrix that reduces the number of flow equations (Nghiem et al., 2004, 2011).

Reactions between the aqueous species and the reactive minerals in a reservoir are kinetically controlled. The reactions involving reservoir minerals cause the minerals to dissolve or precipitate when they are not in a state of equilibrium with the ions in the aqueous phase. The dissolution or precipitation rate of a mineral is calculated as:

$$r_\beta = \hat{A}_\beta k_\beta \left(1 - \frac{Q_\beta}{K_{eq,\beta}}\right), \beta = 1,..., R_{mn} \tag{11}$$

where:

$\hat{A}_\beta$ = reactive surface area of reactant mineral β per unit bulk volume of porous medium (m^2/m^3)

k_β = rate constant of mineral reaction β ($mol/m^2 \cdot s$).

$K_{eq,\beta}$ = chemical equilibrium constant of mineral dissolution/precipitation reaction

Q_β = activity product of mineral β dissolution reaction

r_β = dissolution/precipitation rate per unit bulk volume of porous medium [$mol/(m^3 \cdot s)$]

R_{mn} = number of mineral reactions

The reaction rates are normally stated at a reference temperature. The reaction-rate constant k_β at any desired temperature can be found using the following equation:

$$k_\beta = k_{0,\beta} \exp\left[-\frac{E_a}{R}\left(\frac{1}{T} - \frac{1}{T_0}\right)\right] \tag{12}$$

where E_a is the activation energy for reaction (J/mol), $k_{0,\beta}$ is the reaction-rate constant for reaction at reference temperature, R is the universal gas constant (8.314 J/(mol K)), T is the temperature (K) and T_0 is a reference temperature (K).

The reactive surface area of a mineral per unit bulk volume of a porous medium changes as the mineral dissolves or precipitates. Nghiem et al. (2004) employed the following equation to adjust the reactive surface area of a mineral:

$$\hat{A} = \hat{A}_0 . \frac{N_\beta}{N_{\beta 0}} \tag{13}$$

where $\hat{A}_0$ is the reactive surface area at time zero, N_β are the moles of mineral β per grid block volume at current time, and $N_{\beta 0}$ are the moles of mineral β per grid block volume at time zero.

Ion Exchange

In a reservoir environment, there is a chemical equilibrium between ions in the solution and ions that sorb on the mineral surface, mainly on clay. As water with ion concentration different from the connate water ion concentration is injected, ion exchange reactions occur. In a LSW process, two typical ion exchange reactions that involve sodium, calcium and magnesium ions are:

$$Na^+ + \frac{1}{2}(Ca - X_2) \leftrightarrow (Na - X) + \frac{1}{2}Ca^{2+} \tag{14}$$

$$Na^+ + \frac{1}{2}(Mg - X_2) \leftrightarrow (Na - X) + \frac{1}{2}Mg^{2+} \tag{15}$$

where X denotes the clay mineral in the reservoir rock.

The above reaction is reversible and indicates that Na^+ is taken up by the exchanger and Ca^{2+} and Mg^{2+} are released if we inject high salinity brine into a reservoir, while the reversible is true in LSW or there is a surplus of Ca^{2+} and Mg^{2+}.

The following selectivity coefficients are used to model ion exchanges in the clay surfaces:

$$K'_{Na\backslash Ca} = \frac{\zeta(Na - X)\left[m(Ca^{2+})\right]^{0.5}}{\left[\zeta(Ca - X_2)\right]^{0.5} m(Na^+)} \times \frac{\left[\gamma(Ca^{2+})\right]^{0.5}}{\gamma(Na^+)} \tag{16}$$

$$K'_{Na\backslash Mg} = \frac{\zeta(Na - X)\left[m(Mg^{2+})\right]^{0.5}}{\left[\zeta(Mg - X_2)\right]^{0.5} m(Na^+)} \times \frac{\left[\gamma(Mg^{2+})\right]^{0.5}}{\gamma(Na^+)} \tag{17}$$

where $\zeta(Na - X)$, $\zeta(Ca - X_2)$, and $\zeta(Mg - X_2)$ are the equivalent fractions of Na^+, Ca^{2+} and Mg^{2+} on the exchanger, respectively. The use of the selectivity coefficients in Equations (16) and (17) follows the Gaines-Thomas convention (Gaines and Thomas, 1953). Note that the selectivity coefficients $K'_{Na\backslash Ca}$ and $K'_{Na\backslash Mg}$ are operational variables and not thermodynamic variables like the equilibrium constants.

Modeling Wettability Alteration

The effect of wettability alteration is modeled by shifting the relative permeability curves as schematically shown in Figure 1. Multiple relative permeability tables can be defined for a reservoir rock type, where each table corresponds to one value of a specified interpolant. Typically, two sets of relative permeability curves representing, respectively, low salinity and high salinity conditions are considered and an interpolation between these two curves is carried out. The interpolant is the equivalent fraction of an ion on the rock surfaces. Relative permeability curves are usually measured from laboratory experiments and serve as the input data for numerical simulation. It is shown in the core-flood simulation that the use of Ca^{++} equivalent fraction on the exchanger as the interpolant provides a good match of experimental data.

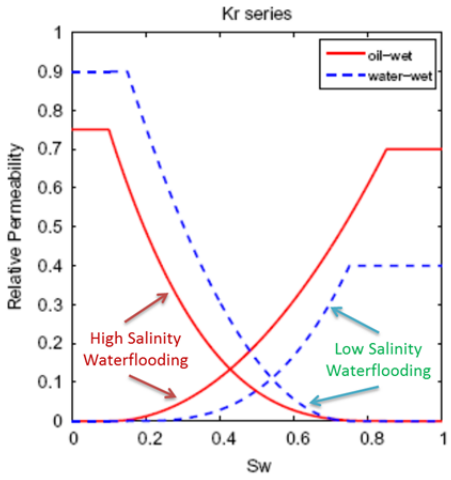

Figure 1: Schematic shifting of relative permeability curves in LSW

Solution Method

The solution method of this model follows Nghiem et al. (2004)'s approach. This method is based on the simultaneous solution of all equations using Newton's method. Let $\vec{\psi}$ be the vector of the material balance equations for all gaseous and aqueous components. Let $\vec{\tilde{\psi}} = E\vec{\psi}$ be the n_c reduced set of the "primary component" material balance equations, where E is an Annihilation matrix. Note that $n_c = n_h + n_a - R_{aq}$. The detailed discussions on the Equilibrium-Rate-Annihilation (ERA) matrix can be found in Nghiem et al. (2004, 2011).

The following equations are taken as the primary equations:

- The volume constraint equation (7),
- The n_c reduced aqueous component material equations $\vec{\tilde{\psi}}$,
- The n_h oil-gas phase equilibrium equations (4),
- The n_h gas-water phase equilibrium (5),
- The R_{aq} chemical equilibrium equations (8),
- The n_m mineral balance equations (3), and
- The n_{ex} ion exchange equations.

In total, there are $(1+ n_c + 2\, n_h + R_{aq} + n_m + n_{ex})$ equations. The primary unknowns are:

- Pressure,
- The summed mole numbers of oil and gas components, N_i, $i = 1,\ldots,n_h$,
- The mole numbers of aqueous components, N_j, $j = 1,\ldots,n_a$,
- The mole numbers of components in the gas phase, N_{ig}, $i = 1,\ldots,n_h$,
- The mole numbers of oil/gas components soluble in the aqueous phase, N_{iw}, $i = 1,\ldots, n_h$,
- The mole numbers of minerals, N_k, $k = 1,\ldots, n_m$,
- The moles of ions on the exchanger, N_e, $e = 1,\ldots, n_{ex}$.

Let $\vec{\psi}$ be the vector comprising all equations for all gridblocks and $\vec{\xi}$ the vector of all primary variables. Then the whole system of equations is solved with Newton's method:

$$\vec{\xi}^{(k+1)} = \vec{\xi}^{(k)} - \left[\left(\frac{\partial\vec{\psi}}{\partial\vec{\xi}}\right)^{(k)}\right]^{-1} \vec{\psi}^{(k)} \qquad (18)$$

where $\left(\frac{\partial\vec{\psi}}{\partial\vec{\xi}}\right)$ is the Jacobian matrix and the superscript (k) denotes the iteration level. The Jacobian matrix is a sparse matrix that is solved by Incomplete LU factorization followed by the GMRES iterative method.

This solution method allows the simultaneous convergence of the flow equations, the phase equilibrium equations, the chemical equilibrium reaction equations, the mineral dissolution and precipitation equations and the ion exchange equations.

Results and Discussions

This section documents the results of validation between this new model and (1) the geochemistry software PHREEQC and (2) laboratory measurements. The PHREEQC software and a series of North Sea sandstone and Texas's reservoir coreflood experiments conducted by Fjelde et al. (2012) and Rivet (2009) served as the basis for this validation. The mechanistic simulations in this section include brine/rock interactions, dynamic single/multiple ion exchange, intra-aqueous reactions, mineral dissolution/precipitation, and CO_2 solubility.

Comparison of Ion Exchange Model with PHREEQC

PHREEQC is designed to perform a wide variety of low-temperature aqueous geochemical calculations and processes in natural water or laboratory experiments. This program is based on equilibrium chemistry of aqueous solutions interacting with minerals, gases, solid solution, exchangers, and sorption surfaces. It could also be used to simulate one-dimensional transport phenomenon with dispersion and diffusion.

The base case for comparison of the ion exchange model developed in this work with that in PHREEQC is based on Appelo's problem (Appelo, 1994). Either a low or high salinity brine slug is used to displace formation water that initially contains sodium and/or calcium chloride solution in equilibrium with the cation exchanger (Figure 2). The aquifer is then flooded with brine that contain sodium chloride and calcium chloride at different concentrations.

Figure 2: Base case simulation for ion exchange validation

The linear model in PHREEQC has 20 cells, and it requires that 20 solutions, numbered 1 through 20, be defined; the number of the solutions corresponds to the number of the cells in the model. In this validation, all cells contain the same solution, and the number of the exchangers corresponds to the number of the cells in a column. In PHREEQC, the ADVECTION data block needs only include the number of cells and the number of shifts for the simulation. The calculation only accounts for the number of pore volumes that flow through the cells with no explicit definition of time or distance.

A one-dimensional linear homogeneous reservoir model that consists of 20 grid blocks with properties shown in Table 2 was used in this comparison. Since this is a displacement of water slug, porosity is set at a value of 0.99. The ion exchange is allocated for all grid blocks with a constant value. This model involves some important geochemistry reactions during LSW; however, these geochemistry properties are not included in the base case simulation.

We use the low salinity injected brine to displace formation water as shown in Table 3. The evolution between Ca^{2+} and Na^{+} in the effluent from GEM™ and PHREEQC are plotted in Figure 3. There is a very good match between GEM™ and PHREEQC. These results are also consistent with the analytical results by Appelo (1994) using mass balance over the front. Initially, the effluent is in equilibrium with the original exchanger composition, formation water is produced until 0.7 of injected pore volume, and then the fronts have a sharpening tendency because of a preference for the displacing ions.

Table 2: Basic Reservoir Properties for Base Case

Parameter	Value for Base Case
Grid blocks system	20 x 1 x 1
Grid block sizes	Δx = 3.66 m, Δy = 30.48 m, Δz = 15.24 m
Horizontal permibilities	2000 mD
Vertical permeabilities	2000 mD
Porosity	0.99
Ion exchange	$\frac{1}{2}Ca^{2+} + Na\_X \leftrightarrow \frac{1}{2}Ca\_X_2 + Na^{+}$
CEC	50
Selectivity coefficient	0.4 at 25°C (From Appelo, 1994)

Table 3: Brine Composition Used for Low Salinity Waterflooding

	Na^+	Ca^{2+}	Cl^-
Injected Brine (mol/l)	0.01326	0.000148	0.01622
Connate Water (mol/l)	1.326	0.148	1.622

The detailed exchange between Na^+ and Ca^{2+} is described in Figure 4. The equivalent fraction of Ca-X_2 increases with a decrease of Na-X, which exactly follows the hypothesis of calcium absorption when low salinity brine is injected into the reservoir:

$$\frac{1}{2}Ca^{2+} + Na - X \leftrightarrow \frac{1}{2}Ca - X_2 + Na^+ \quad (19)$$

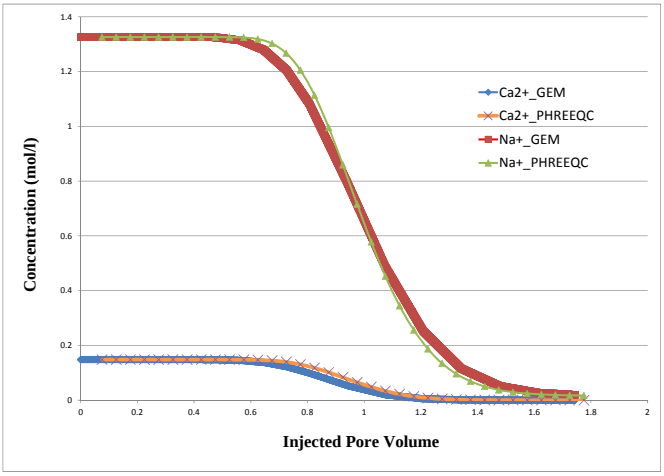

Figure 3: Effluent evolution of Ca^{2+}/Na^+ during LSW - GEM™ vs. PHREEQC

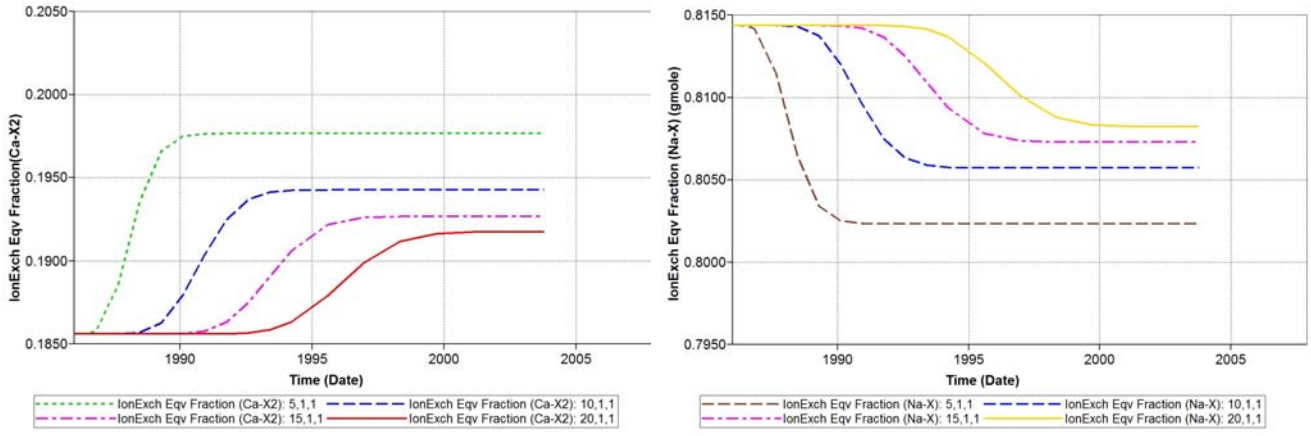

Ca-X_2 **Na-X**

Figure 4: Evolution of the equivalent fractions of Ca-X_2 and Na-X for various gridblocks

The evolution of Ca^{2+} in the high and low divalent ions in formation water (Table 4) was also simulated and compared with PHREEQC. A very good agreement between GEM™ and PHREEQC on the Ca^{2+} effluent after ion exchange (Figure 5) was obtained.

Table 4: Connate Water Composition Used for Evaluating Calcium Ions Effects

	Na^+	Ca^{2+}	Cl^-
High Calcium Connate Water (mol/l)	1.326	0.148	1.622
Low Calcium Connate Water (mol/l)	1.326	0.08	1.486

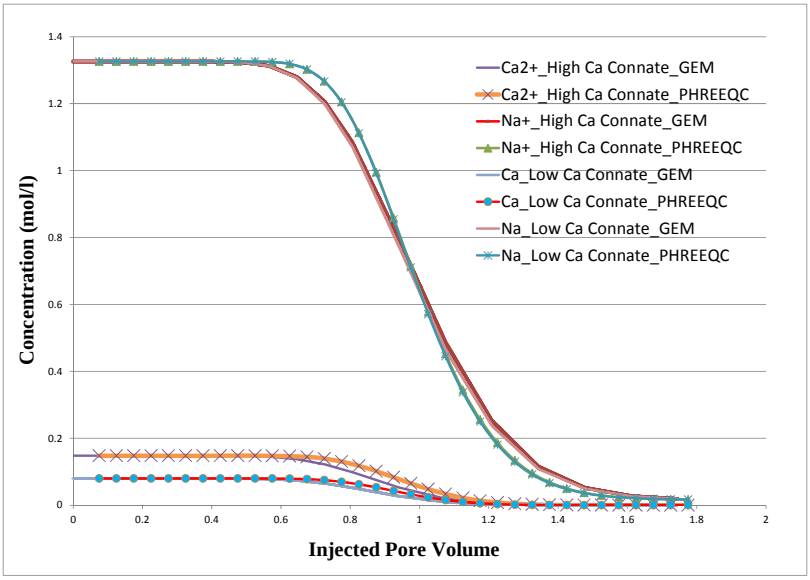

Figure 5: Effluent evolution of Ca^{2+}/Na^{+} for high and low divalent ion in formation water GEM™ vs. PHREEQC

Model Validation with North Sea Coreflood Experiment

Fjelde et al. (2012) reported a systematic experimental study of LSW based on corefloods. The results from this study including formation and injection brine composition, relative permeability curves for high and low salinity waterflooding, evolution of effluent divalent ions, average oil saturation, and pH are used to validate our LSW model.

The compositions and properties of the synthetic formation water (FW), sea water (SW) and low salinity water (LSW) used in the coreflooding experiments are given in Table 5. Core plugs from a sandstone oil reservoir in the North Sea were used in the flooding experiments. The reservoir core plugs were prepared with formation water (FW) and aged with crude oil at initial water saturation (S_{wi}). These core plugs were flooded by FW, sea water (SW), and then low salinity water (LSW). The effluent samples were analyzed for ion concentrations and pH. In all the above flooding experiments, the injection velocity was 6.323 cm/d with about 10 injected pore volumes for each stage.

A one-dimensional model has been setup in order to simulate the above coreflooding experiments. It consists of 40 gridblocks with the same properties as the sandstone core in Fjelde et al.'s experiment. The clay content in the rock was about 13% weight of the bulk sample and the important reservoir properties are listed in Table 6. In this model, we considered the reversible ion exchange between calcium and sodium as well as aqueous and mineral reactions.

The reactions that are modeled are:

$$CO_2(aq) + H_2O \leftrightarrow H^+ + HCO_3^- \quad (20a)$$

$$H^+ + OH^- \leftrightarrow H_2O \quad (20b)$$

$$\text{Calcite} + H^+ \leftrightarrow Ca^{2+} + HCO_3^- \quad (20c)$$

$$\frac{1}{2}Ca^{2+} + Na - X \leftrightarrow \frac{1}{2}Ca - X_2 + Na^+ \quad (20d)$$

The dissolution of calcite is one of the most important reactions in LSW. It provides a Ca^{2+} source for ion exchange that affects the reservoir wettability. Buckley et al. (1998), Lebedeva and Fogden (2010), and Suijkerbuijk et al. (2012) indicated that the Ca^{2+} concentration is important in determining wettability and the relative permeability curves depends on formation brine composition. In the one-dimensional model, we used two

relative permeability sets that were provided by Fjelde et al. (2012).

Table 5: Brine Composition Used for Coreflood Experiments (Fjedel et al., 2012)

	Formation Water (FW) (mol/l)	Sea Water (SW) (mol/l)	Low Salinity Waterflooding (LSW) (mol/l)
Na^+	1.32622	0.45011	0.01326
Ca^{2+}	0.14794	0.01299	0.00148
Mg^{2+}	0.01746	0.04451	0.00018
Cl^-	1.67773	0.52513	0.01661
SO_4^{2-}	0.00089	0.02401	0.00001
K^+	0.00562	0.01006	0.00006
HCO_3^-	0.000118	-	-

Table 6: Basic Reservoir Properties for Run 2

Grid blocks system	40 x 1 x 1
Grid block sizes	$\Delta x = 0.2$ cm, $\Delta y = 2$ cm, $\Delta z = 3.8$ cm
Horizontal permibilities	150 mD
Vertical Permeabilities (mD)	150 mD
Porosity	0.279
Volume of Clay	0.13
Injection Velocity	6.323 cm/d

Dynamic Ion Exchange

There are three stages of injection including formation water injection, sea water injection, and low salt water injection. Calcium ions are expected to exchange with sodium ions on the clay surface. We compare the evolution of effluent Ca^{2+} concentration from experimental measurements and from the simulator GEM™. To examine the effect of ion exchange, two GEM™ runs were performed. In the first run, ion exchange was not included in the simulation. Figure 6 shows a good agreement between simulation and experimental results during the first injection stage with formation water. However, the simulated concentration of Ca^{2+} is lower than that in the experiments when the injected fluid switches from formation water into sea water and then to low salinity water. The calcium concentration was constant at the injected concentration value. This discrepancy is due to the absence of ion exchange consideration in different injected modes.

A much better match for sea water and low salinity water injection stages could be obtained when the model includes the reversible ion exchange reactions, cation exchange capacity of clays, the amount of the clay in the rock, the concentrations of the cation, and the selectivity coefficients. Figure 7 shows an excellent match of the effluent calcium evolution between GEM™ with ion exchange and the experimental results.

Figure 8 shows the dynamic ion exchange process inside the core for the experiment described above. The equivalent fraction of $Ca\text{-}X_2$ is constant during the first 10 injected pore volumes of FW because of the invariable of the ion concentrations between the injected brine and formation water. Then the Ca^{++} adsorbs on the clay minerals when FW injection was switched to SW injection with a significant reduction of salinity concentration (Figure 8a). It is important to note that the injected Ca^{++} concentration in the Fjelde et al.'s experiment is very low, leading to the desorption of Ca^{++} after the formation water had been flushed out at about 11 injected pore volumes. The relative low Ca^{++} concentration in the injection SW causes the variation of ion exchange along the core sample. The ion exchange is reduced and the values of $Ca\text{-}X_2$ are higher in the last blocks after 20 injected PVs of SW injection. Based on the simulation results these differences on the ion exchange equivalent fraction could be explained with an extended SW injection as shown in Figure 8b (i.e. 20 PV SW injection).

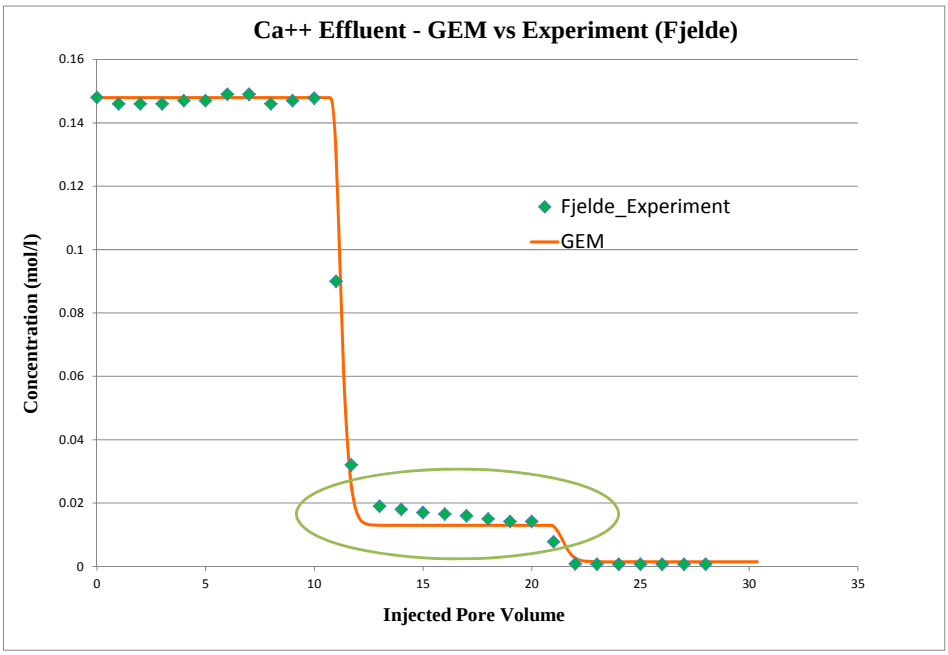

Figure 6: Evolution of Ca^{2+} without ion exchange vs. experimental coreflooding (Fjelde et al., 2012)

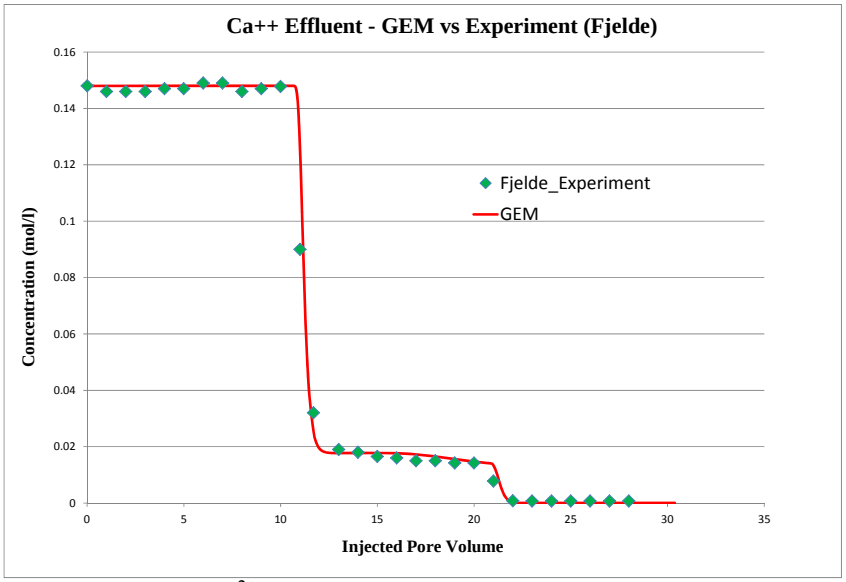

Figure 7: Evolution of Ca^{2+} - GEM™ vs. experimental coreflooding (Fjelde et al., 2012)

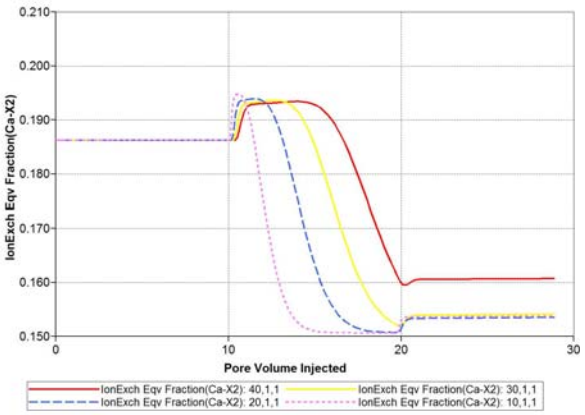

a. Ca-X_2

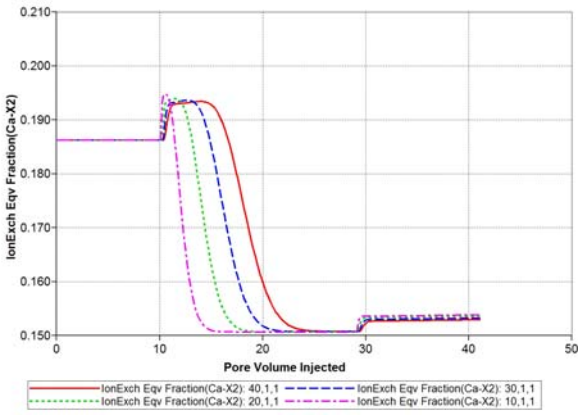

b. Ca-X_2 (Extended SW Injection)

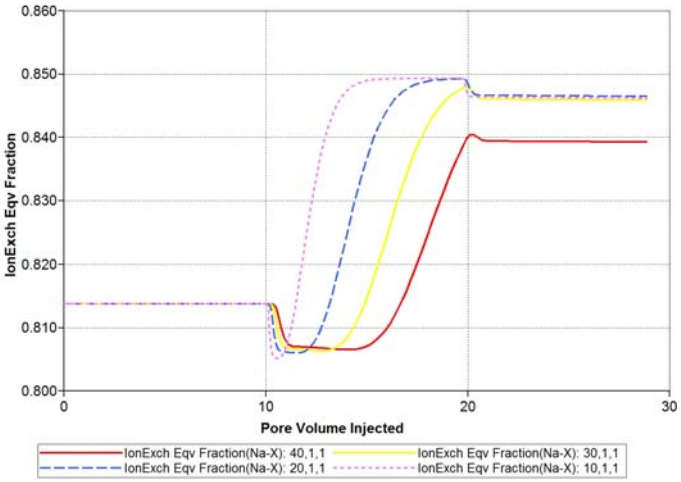

c. Na-X

Figure 8: Evolution of equivalent fraction Ca-X_2/Na-X inside core sample

pH Profile

Without ion exchange and geochemical reactions, the simulation is not able to capture the change in pH during LSW. Figure 9 shows an excellent match of the effluent pH when using ion exchange coupled with geochemistry in LSW. The new model can match well the variance in the effluent pH that increases as the injected brine salinity decreases. Several researchers observed the same trend of an increase in the effluent pH during LSW (McGuire et al., 2005; Lager et al., 2006; Austad et al., 2010). McGuire (2005) concluded that the local pH increase in LSW is relatively similar to the mechanisms in alkaline flooding and it may contribute to the additional oil recovery. However, a pH increase is not the main mechanism responsible for high oil recovery by LSW since pH is only 1 to1.5 units higher than the injected pH and the final pH value is much smaller than the one in alkaline flooding. The small increase in pH is doubtful to produce a sufficient amount of in-situ surfactant as McGuire et al.'s conclusion (RezaeiDouts et al. 2009, Melberg., 2010). A local pH increase during the LSW process can be explained by the dissolution of calcite minerals as shown by reaction (20c). The aqueous phase lost protons as soon as the calcite mineral starts to dissolve, leading to an increase in the effluent pH.

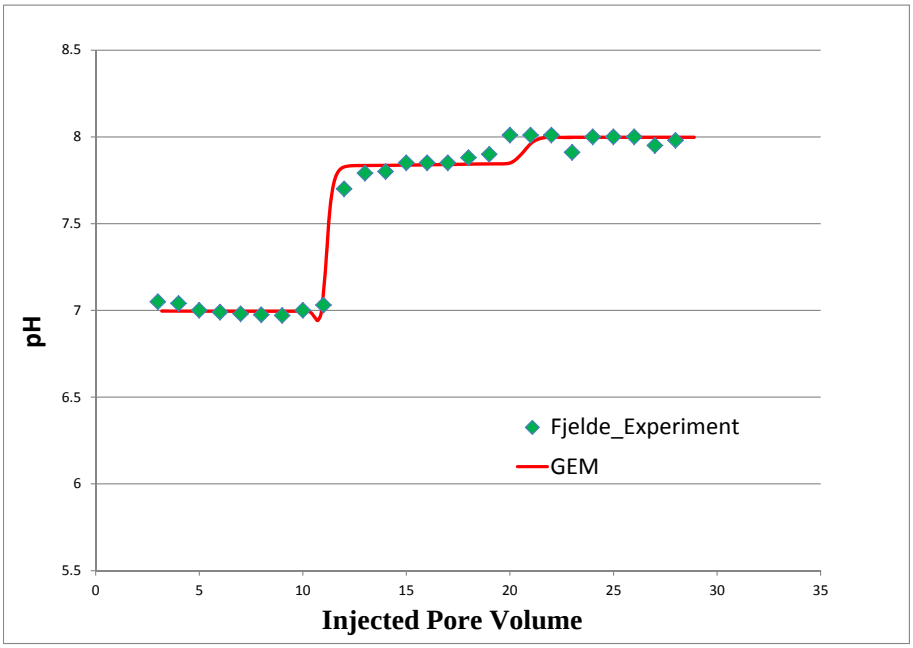

Figure 9: pH - GEM™ vs. experimental coreflooding (Fjelde et al., 2012)

Effects of Wettability Alteration

Without ion exchange and its effect on wettability, the simulation cannot capture the LSW effect and leads to a difference between the average oil saturation prediction and measured values as shown in Figure 11. The experiment data clearly show a decrease in the average oil saturation with LSW. However, the average oil saturation in simulation is constant even when injection was changed from formation water injection to sea water injection and low salinity water injection.

Since the concentration of Ca^{++} in the connate water has a strong effect on the oil and water relative permeabilities (Dang et al. 2013., Suijkerbuijk et al. 2012., Rivet. 2009, Buckley et al. 1998), the equivalent fraction of Ca-X_2 which represents the exchangeable amount of Ca^{++} is used as the interpolant for the wettability alteration due to LSW effects. An excellent match of oil saturation could be obtained with wettability alteration as a result of ion exchange and the two experimentally determined relative permeability sets from the work of Fjelde et al. (2012) for high/low salinity waterflooding. The adsorption of Ca^{++} leads to the wettability alteration towards more water wetness and is responsible for the additional oil recovery. The equivalent fraction of Ca-X_2 increases as SW injection is switched to LSW. However this change is relative small with a minor effect on the oil recovery. This observation strongly supports for our hypothesis: the absorption of Ca^{++} leads to a modification of relative permeabilities, resulting on a higher oil recovery.

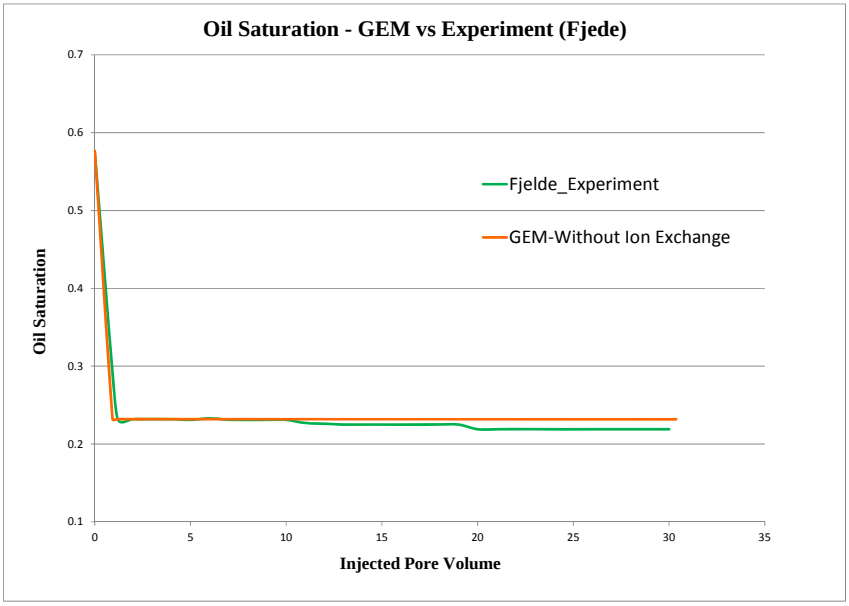

Figure 11: Oil Recovery - GEM™ (without modeling of wettability alteration) vs. experimental coreflooding (Fjelde et al., 2012)

Most of the oil was produced at the initial time during FW injection. The oil saturation after FW injection is around 24.5% and it further deceased to 23.5% during sea water injection. By interpolating between the two relative permeability curves based on the net ion exchange, an excellent match of oil saturation was obtained.

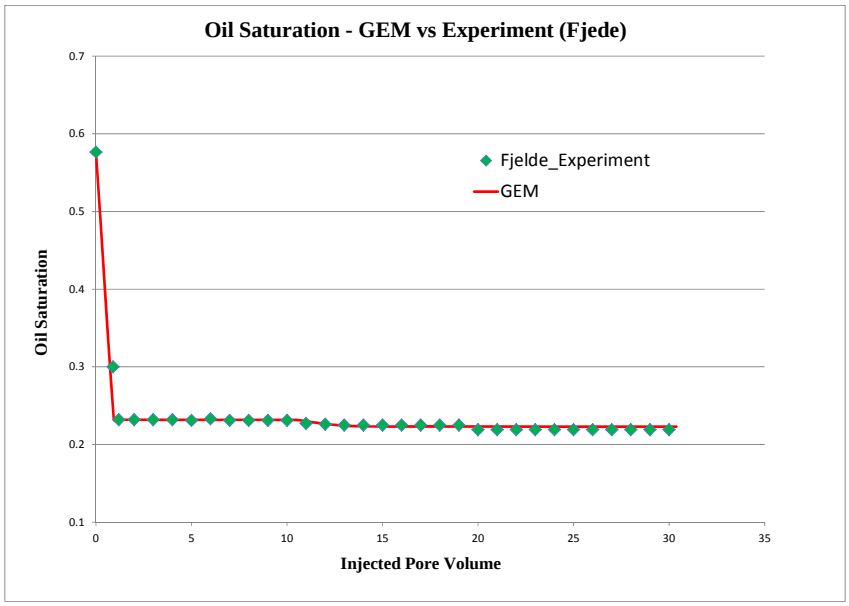

Figure 12: Average oil saturation - GEM™ vs. experimental coreflooding (Fjelde et al., 2012)

Model Validation with Sandstone Reservoir Core-Flood Experiment

Rivet (2009) presented a series of core floods on Berea and reservoir sandstone core samples with high and low salinity brines to study the effect of salinity on oil recovery, residual oil saturation and relative permeability. In these experiments, the core is composed of 6 core plugs that were taken from an unconsolidated sandstone oil reservoir. The plug arrangement into the core is such that air permeability decrease towards the core outlet. These plugs have an average clay content of about 20 wt% based on the XRD analysis. Plug properties are given in Table 6.

Table 6: Rivet's Core Property

Plug Number	Porosity (%)	K_{air} (mD)	Length (cm)
1-1	26.5	338	4.8
1-2	26.3	379	4.8
1-3	26.7	469	5.0
1-4	27.8	634	5.0
1-5	27.5	665	4.8
1-6	25.1	888	5.1

Two brines were used during the waterflood experiments: Synthetic Reservoir Formation Brine (SRCFB), with 31,000 ppm TDS as the high salinity brine and Synthetic Lake C Water (SLCW), with 1,075 ppm TDS as the low salinity brine. Fluid properties are given in Table 7.

Table 7: Fluid Properties for Rivet's Core-Flood Experiments

SRCFB Concentration (g/L)	28.62 NaCl 0.65 KCl 2.71 $CaCl_2$ 3.89 $MgCl_2$-$6H_2O$
SLCW Concentration (g/L)	0.7 NaCl 0.21 $CaCl_2$ 0.35 $MgCl_2$-$6H_2O$

A one-dimensional model has been setup to simulate the above core-flood experiments. The model consists of 60 grid blocks, representing the six plugs in Rivet's core sample with the reservoir properties shown in Table 8. Two sets of relative permeability curves provided by Rivet (2009) were used for simulating the LSW effects.

Table 8: Basic Reservoir Properties for Run 3

Grid blocks system	60 x 1 x 1
Absolute permibilities	10*338 mD, 10*379 mD, 10*469 mD, 10*634 mD, 10*665 mD, 10*888 mD
Porosity	10*0.265, 10*0.263, 10*0.267, 10*0.278, 10*0.275, 10*0.251
Volume of Clay	0.2
Injection Velocity	60.9 cm/d

Figure 13 shows the comparison results on the average oil saturation between the model without ion exchange and the new LSW model with ion exchange and wettability alteration versus the experimental data provided by Rivet. The average oil saturation decreases from 0.6 to 0.235 by LSW. The LSW in Rivet's experiment has a better effect on oil recovery in comparison with the one in Fjelde et al.'s experiment because of better injected brine composition. Figure 14 indicates that the ion exchange reaction support the hypothesis that calcium ions adsorb on the rock surface, resulting in an increase of the oil relative permeability and a decrease of water relative permeability as experimentally shown by Rivet (2009). The ion exchange during LSW, therefore, contributes to the alteration of wettability towards more water wetness, and thus to the additional oil recovery. With the new proposed LSW model, an excellent history match for both high salinity and low salinity waterflood experiments from the work of Rivet (2009) could be achieved as shown in Figures 15 and 16.

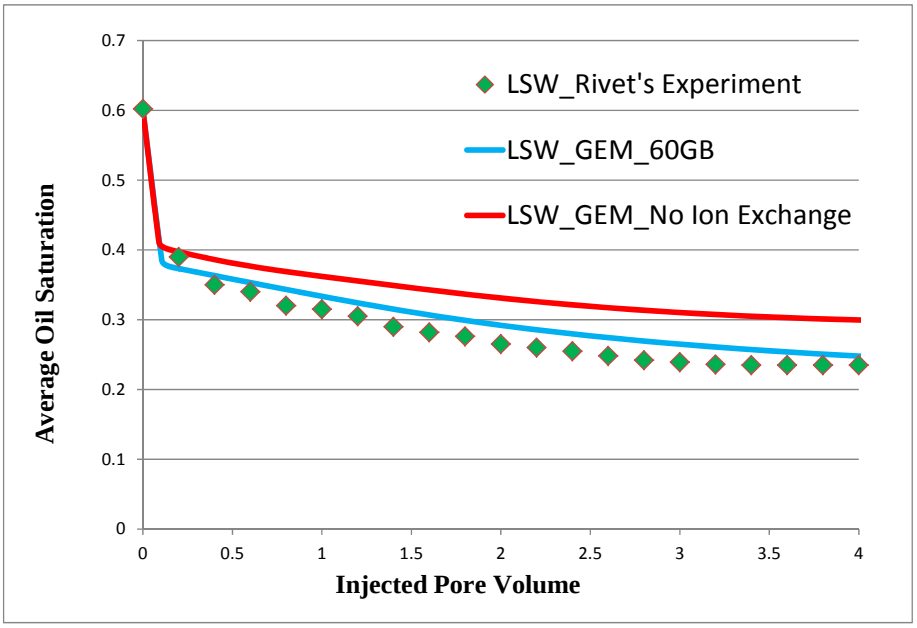

Figure 13: Average oil saturation - GEM™ vs. experimental coreflooding (Rivet, 2009)

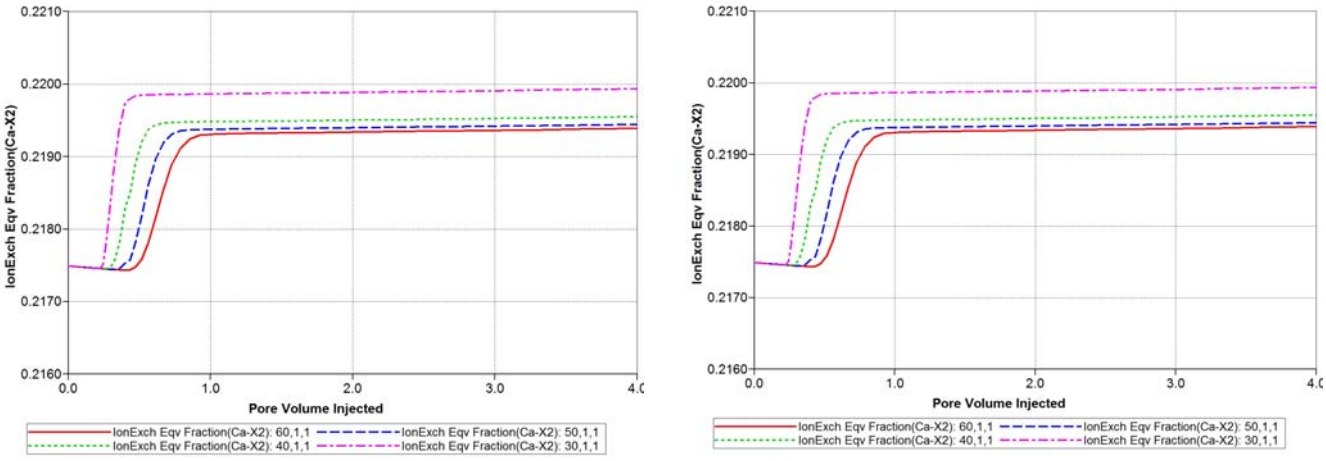

$Ca\text{-}X_2$ Na-X

Figure 14: Evolution of equivalent fraction $Ca\text{-}X_2$/Na-X inside core sample

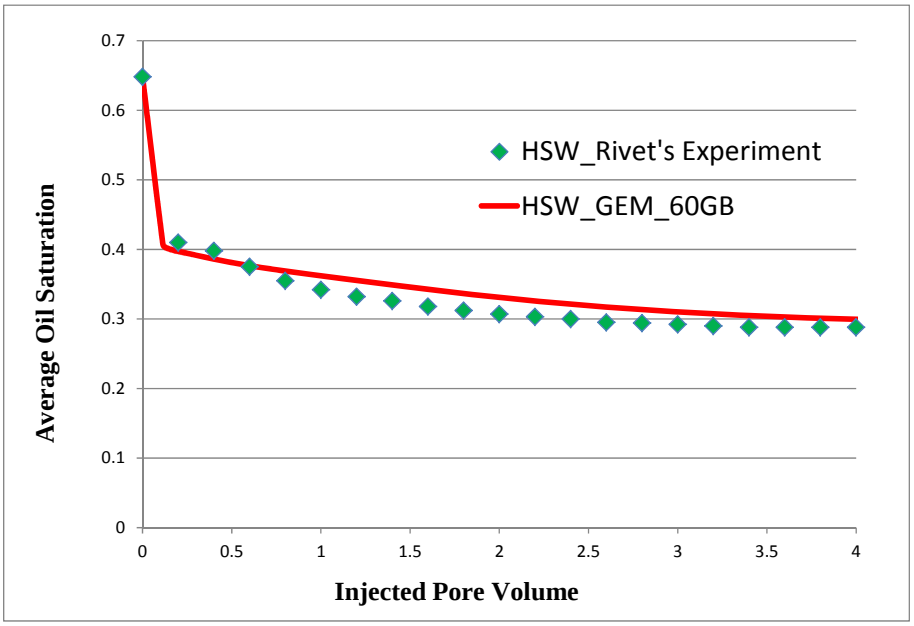

Figure 15: Average oil saturation – HSW: GEM™ vs. experimental coreflooding (Rivet, 2009)

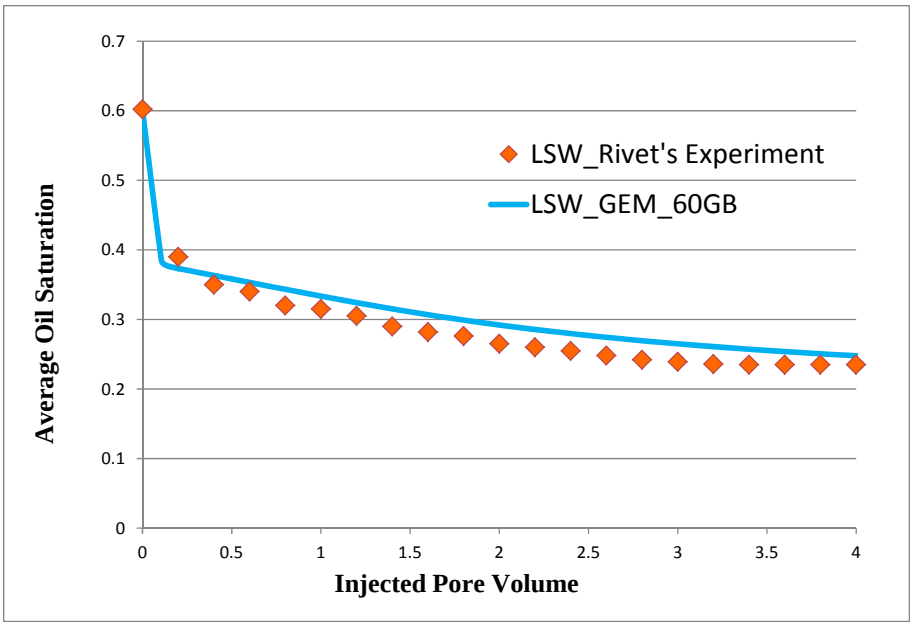

Figure 16: Average oil saturation – HSW: GEM™ vs. experimental coreflooding (Rivet, 2009)

The pH effluent profiles between the LSW model and Rivet's experimental data are compared in Figure 17. The pH was initially decreased from 7.1 to 6.3 because of calcite precipitation. As long as low salinity brine was continuously injected into the core sample, the pH effluent tended to increase due to the dissolution of the calcite and ion exchange effect.

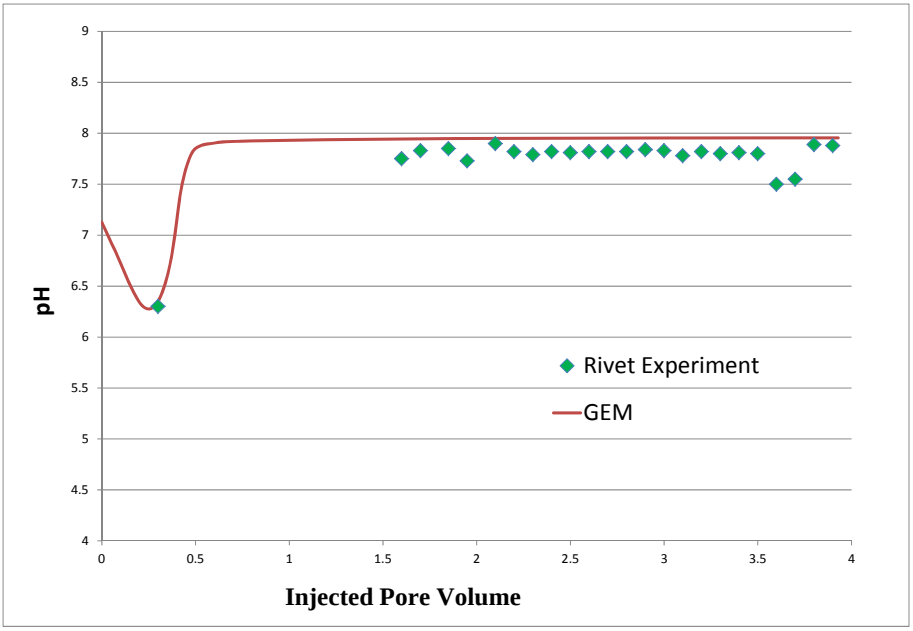

Figure 17: Effluent pH history – GEM™ vs. experimental coreflood (Rivet, 2009)

Conclusions

LSW is an important EOR technique as it shows more advantages than conventional chemical EOR methods in terms of chemical costs, environmental impact, and field process implementation. This paper presents a method for modeling this process. A comprehensive ion exchange model with geochemistry has been developed and coupled to the multi-phase multi-component flow equations in an equation-of-state compositional simulator. This new model captures most of the important physical and chemical phenomena that occur in LSW, including intra-aqueous reactions, mineral dissolution/precipitation, and wettability alteration.

The new model was successfully validated with (1) the ion-exchange model of the geochemistry software PHREEQC, (2) the low-salinity core-flood experiments for a North Sea reservoir, and (3) the low salinity and high salinity heterogeneous core-flood experiments for a Texas reservoir. Excellent agreements were obtained on the evolution of ions in (1), which validates the ion-exchange and geochemistry model. For (2) and (3), excellent matches of experimental effluent ion concentrations, effluent pH and oil recovery were also obtained, which show that the proposed model can capture the main mechanisms of LSW. It is shown in the core-flood simulation that the use of Ca^{++} equivalent fraction on the exchanger as the interpolant is sufficient to provide a good match of experimental data. This applies only for the cases considered in this paper. Additional investigations are being conducted to examine situations where Mg^{++} equivalent fraction would also play a role.

Important observations in the laboratory and field tests such as a local pH increase, a decrease in divalent effluent concentration, mineralogy contributions, and the influence of connate water/injected brine compositions can be fully explained from the proposed LSW model. Built in a robust reservoir simulator, it serves as a powerful tool for LSW design and the interpretation of process performance in the field.

Acknowledgements

The authors thank Dr. Vijay Shrivastava of Computer Modelling Group Ltd. for his valuable comments.

Nomenclature

a_i = activity of component i

$\hat{A}_\beta$ = reactive surface area of mineral β

d = depth

D_{iq} = dispersion coefficient in phase q (q = g, o, w)

E_a = activation energy

E = Equilibrium-Rate-Annihilation (ERA) matrix

g = gravity acceleration

H_i = Henry's law constant of component i
K = permeability
K'= selectivity coefficient
k_β = reaction rate constant of mineral reaction β
K_{eq} = chemical equilibrium constant
m_i = molality of component i
n_a = number of aqueous components
n_{ct} = total number of components
n_h = number of hydrocarbon components
n_g = number of gaseous components
n_o = number of oleic components
n_i = moles of component i
P = pressure
q_i = injection/production rate of component i
Q_β = activity product
r_β = reaction rate of mineral β
R_{aq} = number of reactions in aqueous phase
R_{mn} = number of mineral reactions
S = saturation
T = Temperature
T_q = molar transmissibility of phase q (q = o, g, w)
V = gridblock bulk volume
y_{iq} = mole fraction of component I in phase q (q = o, g, w)
Δ = difference operator
φ = porosity
γ_i = activity coefficient of component i
$\nu_{k\alpha}$ = stoichiometric coefficient of a species for the chemical reaction
$\tilde{\rho}$ = mass density
σ = reaction rate
ζ = ion exchange equivalent fraction
$\vec{\xi}$ = vector of primary variables
ψ = constitutive equation
$\vec{\psi}$ = vector of constitutive equations

Reference

1. Appelo, C.A.J. 1994. Cation and Proton Exchange, pH Variations, and Carbonate Reactions in a Freshening Aquifer. Water Resources Research Journal, 30(10):2893-2805.
2. Bethke, C.M. 2006. GWB Essentials Guide. University of Illinois May 4.
3. Buckley, J.S., Liu, Y., Monsterleet, S. 1998. Mechanisms of Wetting Alteration by Crude Oils. Paper SPE 37230 presented at the SPE International Symposium on Oilfield Chemistry, Houston, TX, USA, 18-21 February.
4. Buckley, J.S., Morrow, N.R. 2010. Improved Oil Recovery by Low Salinity Waterflooding: A Mechanistic Review. Paper presented at 11th International Symposium on Evaluation of Wettability and Its Effect on Oil Recovery, Calgary, 6-9 September.
5. Dang, T.Q.C., Nghiem, L.X., Chen, Z., Nguyen, T.B.N. 2013. State-of-the Art Smart Low Salinity Waterflooding for Enhanced Oil Recovery. Paper SPE 165903 presented at the 2013 SPE Asia Pacific Oil & Gas Conference and Exhibition, Jakarta, Indonesia, 22-24 October.
6. Fjelde, I., Asen, S.V., Omekeh, A. 2012. Low Salinity Water Flooding Experiments and Interpretation by Simulations. Paper SPE 154142 presented at the Eighteenth SPE Improved Oil Recovery Symposium, Tulsa, OK, USA, April 14-18.
7. Jadhunandan, P.P., Morrow, N.R. 1995. Effect of Wettability on Waterflood Recovery for Crude-Oil/Brine/Rock Systems. SPE Reservoir Engineering, 10(1):40-46.
8. Jerauld, G.R., Lin, C.Y., Webb, K.J., Seccombe, J.C. 2008. Modeling Low Salinity Waterflooding. SPE Reservoir Engineering, 11(6):1000-1012.

9. Kharaka, Y.K., Gunter, W.D., Aggarwal, P.K., Perkins, E.H., DeBraal, J.D. 1988. SOLMINEQ.88: A Computer Program for Geochemical Modeling of Water-Rock Interactions. US Geological Survey, Water Resources Investigation Report 88-4227, Menlo Park, CA.
10. Kumar, M., Fogden A., Morrow, N.R., Buckley, J.S. 2010. Mechanisms of Improved Oil Recovery from Sandstone by Low Salinity Flooding. Paper SCA 2010-25 presented at the 24th International Symposium of Core Analysts, Halifax, Canada, 4-7 October.
11. Lager, A., Webb, K.J., Black, C.J.J. 2007. Impact of Brine Chemistry on Oil Recovery. Paper A24 presented at the 14th EAGE Symposium on Improved Oil Recovery, Cairo, 22-24 April.
12. Lager, A., Webb, K.J., Black, C.J.J., Singleton, M., Sorbie, K.S. 2006. Low-Salinity Oil Recovery – An Experimental Investigation. Paper SCA 2006-36 presented at the International Symposium of the Society of Core Analysts, Trondheim, Norway, 12-16 September.
13. Lager, A., Webb, K.J., Black, C.J.J., Singleton, M., Sorbie, K.S. 2008a. Low-Salinity Oil Recovery – An Experimental Investigation. Petrophysics 49(1):28-35.
14. Lager, A., Webb, K.J., Collins, I.R., Richmond, D.M. 2008b. LoSal™ Enhanced Oil Recovery: Evidence of Enhanced Oil Recovery at the Reservoir Scale. Paper SPE 113976 presented at the SPE/DOE Improved Oil Recovery Symposium, Tulsa, 19-23 April.
15. Loahardjo, N., Xie, X., Morrow, N.R. 2010. Oil Recovery by Sequential Waterflooding of Mixed-Wet Sandstone and Limestone. Energy & Fuels, 24(9):5073-5080.
16. McGuire, P.L., Chatam, J.R., Paskvan, F.K., Sommer, D.M., Carini, F.H. 2005. Low Salinity Oil Recovery: An Exciting New EOR Opportunity for Alaska's North Slope. Paper SPE 93903 presented at the SPE Western Regional Meeting, Irvine, CA, USA, 30 March-1 April.
17. Morrow, N.R., Bukley, J.S. 2011. Improved Oil Recovery by Low-Salinity Waterflooding. JPT, Distinguished Author Series, 106-112.
18. Morrow, N.R., Tang, G.Q., Valat, M., Xie, X. 1998. Prospects of Improved Oil Recovery Related to Wettability and Brine Composition. Journal of Petroleum and Engineering, 20(3-4):267-276.
19. Nghiem, L.X., Sammon, P., Grabenstetter, J., Ohkuma, H. 2004. Modeling CO2 Storage in Aquifers with Fully-Coupled Geochemical EOS Compositional Simulator. Paper SPE 89474 presented at the SPE Fourteenth Symposium on Improved Oil Recovery, Tulsa, OK, USA, April 17-21.
20. Nghiem, L.X., Shrivastava, V., Kohse, B. 2011. Modeling Aqueous Phase Behavior and Chemical Reactions in Compositional Simulation. Paper SPE 141417 SPE Reservoir Simulation Symposium, The Woodlands, TX, USA, February 21-23.
21. Omekeh A., Friis H.A., Fjelde I., Evje S. 2012 Modeling of Ion-Exchange and Solubility in Low Salinity Waterflooding. Paper SPE 154144 presented at the Eighteenth SPE IOR Symposium, Tulsa, OK, 14-18 April.
22. Rivet, S.M. 2009. Coreflooding Oil Displacements with Low Salinity Brine. Master Thesis, University of Texas at Austin.
23. RezaeiDoust, A., Puntervold, T., Strand, S., Austad, T. 2009. Smart Water as Wettability Modifier in Carbonate and Sandstone: A Discussion of Similarities/Differences in the Chemical Mechanisms. Energy & Fuels, 23(9): 4479-4485.
24. Rueslatten, H.G., Hjelmeland, O., Selle, O.M. 1994. Wettability of Reservoir Rocks and The Influence of Organo-metallic compounds: North Sea Oil and Gas Reservoir. 3:317-324.
25. Seccombe, J., Lager, A., Jerauld, G.R., Jhavier, B., Buikema, T., Bassler, S., Denis, J., Webb, K., Cockin, A., Fueg, E. 2010. Demonstration of Low Salinity EOR at Interwell Scale, Endicott Field, Alaska. Paper SPE 129692 presented at SPE/DOE Improved Oil Recovery Symposium, Tulsa, 24-28 April.
26. Skrettingland, K., Holt, T., Tweheyo, M.T., Skjevrak. 2010. Snorre Low Salinity Water Injection – Core Flooding Experiments and Single Well Field Pilot. Paper SPE 129877 presented at the SPE Improved Oil Recovery Symposium, Tulsa, OK, USA, 24-28 April.
27. Tang, G.Q., Morrow, N.R. 1997. Salinity, Temperature, Oil Composition and Oil Recovery by Waterflooding. SPE Reservoir Engineering, 12(4):269-276.
28. Tang, G.Q., Morrow, N.R. 1999a. Influence of Brine Composition and Fines Migration on Crude Oil/Brine/Rock Interactions and Oil Recovery. Journal of Petroleum Science and Engineering, 24(2-4):99-111.

29. Tang G.Q., Morrow N.R. 1999b. Oil Recovery by Waterflooding and Imbibition – Invading Brine Cation Valency and Salinity. Paper SCA-9911 presented at the 1999 International Symposium of the Society of Core Analysis, Golden, Colorado, USA, 1-4 August.
30. Thyne, G., Gamage, P. 2011. Evaluation of the Effect of Low Salinity Waterflooding for 26 Fields in Wyoming. Paper SPE 147410 presented at the SPE Annual Technical Conference and Exhibition, Denver, Colorado, USA, 30 October-2 November.
31. Vledder, P., Foncesca, J.C., Wells, T., Gonzalez, I., Ligthelm, D. 2010. Low Salinity Waterflooding: Proof of Wettability Alteration on a Field Wide Scale. Paper SPE 129564 presented at the SPE Improved Oil Recovery Symposium, Tulsa, OK, USA, 24-28 April.
32. Webb, K.J., Black, C.J.J., Al-Ajeel. 2004. Low Salinity Oil Recovery – Log-Inject-Log. Paper SPE 89379 presented at the SPE/DOE Symposium on Improved Oil Recovery, Tulsa, 17-21 April.
33. Webb, K.J., Black, C.J.J., Edmonds, I.J. 2005. Low Salinity Oil Recovery: The Role of Reservoir Condition Corefloods. Paper C18 presented at the 13th EAGE Symposium on Improved Oil Recovery, Budapest, Hungary, 25-27 April.
34. Webb, K.J., Lager, A., Black, C.J.J. 2008. Comparison of High/Low Salinity Water/Oil Relative Permeability. Presented at the International Symposium of the Society of Core Analysts, Abu Dhabi, UAE, 29 October – 2 November.
35. Yildiz, H.O., Morrow, N.R. 1996. Effect of Brine Composition on Recovery of Moutray Crude Oil by Waterflooding. Journal of Petroleum Science and Engineering, 14:159-168.
36. Zhang, Y., Xie, X., Morrow, N.R. 2007. Waterflood Performance by Injection of Brine with Different Salinity for Reservoir Cores. Paper SPE 109849 presented at the SPE Annual Technical Conference and Exhibition, Anaheim, CA, USA, 11-14 November.